Mon. Not. R. Astron. Soc. **398,** 350–356 (2009) doi:10.1111/j.1365-2966.2009.15142.x

A southern hemisphere survey of meteor shower radiants and associated stream orbits using single station radar observations

J. P. Younger,[1⋆] I. M. Reid,[1,2] R. A. Vincent,[1,2] D. A. Holdsworth[3] and D. J. Murphy[4]

[1]*School of Chemistry and Physics, University of Adelaide, SA, Adelaide, 5005 Australia*
[2]*ATRAD Pty. Ltd., 1/26 Stirling St., Thebarton, SA, 5031 Australia*
[3]*ISRD, DSTO, PO Box 1500, Edinbugh, SA, 5111 Australia*
[4]*Australian Antarctic Division, Channel Highway, Kingston, TAS, 7050 Australia*

Accepted 2009 May 26. Received 2009 May 1; in original form 2009 February 13

ABSTRACT

The 33.2 MHz interferometric meteor radars located at Davis Station, Antarctica and Darwin, Australia typically detect around 15 000 specular underdense meteor echoes every day. While the angle of arrival of the scattered radio wave can be inferred using phase differences between receive antennae, the direction of individual meteors is not known beyond a plane of ambiguity perpendicular to the angle of arrival. Using the great circle mapping technique with a Jones & Jones type weighting function, 37 meteor shower systems were detected in data collected at both locations over 2006–2007, including nine undocumented showers. The orbital elements of the parent debris streams were then calculated for the 31 showers where sufficiently precise measurements were available.

Key words: techniques: radar astronomy – surveys – ephemerides – interplanetary medium.

1 INTRODUCTION

Meteor showers are the result of streams of debris orbiting the Sun that collide with the Earth. Travelling in parallel trajectories, the paths of individual meteoroids appear to radiate from a particular point in the sky when seen from the ground, hence the term 'radiant' to describe the direction of a shower's direction of approach to Earth.

Knowledge of a meteor shower's direction and velocity allows the orbit of the parent stream to be determined, which can lead to an association with the parent body that originally produced the debris. At the very least, these parameters contribute to a better understanding of the distribution of material in the Solar system.

From a utilitarian standpoint, even small objects can pose a significant threat to spacecraft, given intercept velocities in excess of 11 km s^{-1}. Collisions with meteoroids were responsible for the loss of the Mariner 4 probe in 1967 (Dycus & Richardson 1969) and the loss of the Olympus communications satellite in 1993 was likely due to a Perseid meteoroid strike (Caswell, McBride & Taylor 1995). Awareness of the locations of hypervelocity meteoroid streams is crucial to future space vehicle design and operational planning.

Traditionally, meteor showers have been detected by visual means, either by employing teams of observers or cameras set up to watch the night sky. The introduction of purpose-built meteor radars in the 1950s made it possible to detect and study ablating meteors during the day and in inclement weather (McKinley 1961). Early radar surveys of meteor activity, such as those by Davies & Gill (1960) and Weiss (1958), focused on overall meteor detection rates and mapping the diffuse radiant distribution of the major sporadic meteor sources.

More recently, specialized radars for detecting the trajectory of individual meteors have been constructed, including the Advanced Meteor Orbit Radar (Baggaley et al. 1994) and the Canadian Meteor Orbit Radar (Jones et al. 2005). These systems have the advantage of producing precise trajectories for individual meteors, but require multiple coordinated stations for triangulation.

More commonly deployed are single station interferometric meteor radars, whose primary mission is to study the properties of the atmosphere through which meteors pass. While these systems are not able to distinguish the trajectory of individual meteors, statistical methods can be implemented to recover the distribution of radiants from a particular data set, providing an opportunity to use data not originally intended for astronomical purposes.

This paper presents the results a survey of narrow meteor shower sources conducted using single station observations. The analysis of 2 yr of data collected at two southern hemisphere sites yielded a number of previously undocumented showers, which are presented alongside the detections of a number of well-known showers to provide an indication of the method's sensitivity. Where possible, meteor shower detections were used to calculate the orbital parameters of the parent streams.

2 METEOR RADAR

Two 33.2-MHz meteor radars were used in this study: one located at Davis Station, Antarctica (69°S, 78°E) and another located at

⋆E-mail: joel.younger@adelaide.edu.au

Darwin, Australia (12°S, 131°E). Both radar receiving antenna arrangements are of five-element interferometer configurations (Jones, Webster & Hocking 1998), with the only difference being the use of dipole antennae on the Davis radar, as opposed to Darwin's cross-dipole antennae. This results in a decrease in sensitivity along the Davis antennae's dipole axis, but for the purposes of shower detection the movement of the entire field of view due to Earth's rotation mitigates this to an extent.

Transmission is via a crossed dipole antenna, effectively providing all-sky coverage. The Gaussian shaped pulses are transmitted with circular polarization (O-mode) at a pulse repetition frequency of 430 Hz with a peak power of 7.5 kW. Signal strength is sampled at a rate of 1.37 MHz during the pulse repetition interval (Holdsworth et al. 2007b). The receive array consists of five antennae in a cross layout, with two pairs of antennae spaced at 2.0 and 2.5 wavelengths from a central antenna along perpendicular baselines (Holdsworth, Reid & Cervera 2004). Angle of arrival is estimated from the phase differences in antennae pairings of 2.5λ and 2.0λ antennae and the central antenna (Holdsworth 2005).

Data acquisition takes place on a Windows NT based PC. Raw data is then transferred to a Linux based PC for the automated detection process. For detected meteors, velocity is estimated using the Fresnel transform technique on the raw phase and amplitude information from the meteor's echo (Elford 2004; Holdsworth et al. 2007). Individual meteor detection details are then stored for further analysis.

The primary purpose of the radars is to study the background winds and variations in the ambipolar diffusion coefficient, which is proportional to T^2/p, where T is temperature and p is pressure. Meteors are detected in an approximately Gaussian height shaped region centred at about 90 km, extending 10–15 km above and below.

The radar specifically looks for underdense meteors, which have sufficiently low-electron densities as to permit coherent, continuous scattering throughout the body of the ionized trail. These are immediately recognizable by their characteristic exponential decay, the decay constant of which is a function of the local ambipolar diffusion coefficient. A result of the scattering mechanism is that the underdense meteors produce highly specular reflections, making them detectable to radar only when the trail's axis is perpendicular to the radar's line of sight (McKinley 1961).

3 LOCATING SHOWER RADIANTS

Due to the specular reflection condition of the meteors detected by interferometric radar, the velocity vector of any given meteor is not known beyond a plane of ambiguity normal to the echo wavefront's angle of arrival. Jones & Jones (2006) provide a detailed description of a statistical method to overcome this limitation, and indeed how to exploit it for the purposes of locating the direction of meteor showers with a single radar station's data.

As a stream of meteoroids collides with the Earth, the possible locations of specular detections will form a great circle across the celestial sphere perpendicular to the stream's direction. To locate these arcs of increased detection activity, a band of sky centred on the arc perpendicular to a radiant of interest is considered. The relative activity of meteors arriving from the radiant of interest is described as the density of detections in the acceptance band, convolved with some weighting function. Following the successful application demonstrated by Holdsworth et al. (2007b), a Jones & Jones filter given by

$$w(\theta) = \begin{cases} 1 - 6\left(\frac{\theta}{\delta\theta}\right)^2 + 5\left(\frac{\theta}{\delta\theta}\right)^4 & \text{for } |\theta| \leq \delta\theta \\ 0 & \text{for } |\theta| > \delta\theta \end{cases} \quad (1)$$

with $\delta\theta = 4^\circ$ was used, where θ is the angular separation to the centre of the acceptance band.

The use of a polynomial weighting function with negative side bands alleviates the diffuse halo effect which occurs with a top-hat type weighting (Holdsworth et al. 2007b). The choice of $\delta\theta$ is based on the angular accuracy of the radar ($\sim 2^\circ$) and the expected width of a narrow meteor stream (1–2°) (Jones & Jones 2006).

A simple discriminator can be used to remove some of the spurious meteor detections from the acceptance band. A particular great circle will be all points perpendicular to a given radiant, but will also be perpendicular to that radiant's mirror. To determine the sense of a single meteor's possible radiant vectors, only detections for which the radar's zenith is in the same hemisphere as the radiant of interest are used. If the radar's zenith was not in the same hemisphere as a trial radiant at the time of detection, it would mean that the meteor was travelling up from the ground (Jones & Jones 2006).

4 SURVEY RESULTS

Two sets of observations collected at Darwin, Australia and Davis Station, Antarctica from 2006–2007 were evaluated for possible shower activity. In total, the data consisted of 6 494 030 events observed over 727 days at Davis Station and 8 800 600 events observed over 605 days at Darwin. Each event represents an unambiguous underdense meteor detection, as recognized by the distinctive exponential decay of echo strength with time. While the data were concentrated in the southern hemisphere, detections recorded at Darwin were seen at declinations as high as $+50^\circ$.

The detections from each location were separated into 24-hr data sets and converted to equatorial (J2000) coordinates. The great circle method was applied to possible radiants spaced at $\sim 1^\circ$ of arc on the celestial sphere, the result being an array of relative activities at each point. The term relative activity is used instead of count, because the implementation of the Jones & Jones filter in the convolution, as opposed to a top-hat type function, does not produce a true count. Indeed, the application of the Jones & Jones filter in practice can result in small negative activities that, while unphysical, do not adversely affect the method's ability to locate narrow regions of elevated activity (Jones & Jones 2006).

The sporadic background produces a distribution of low-activity radiants, but showers show up as outliers on the histogram with much higher activity. It was found that the histogram of positive, non-zero radiant activities generated for all radiants in a single day's data closely approximated a Gaussian distribution. Background noise was defined as 2.5 widths of the Gaussian curve fit to this activity histogram. After some experimentation with different values, a detection threshold of signal-to-noise ratio = 2.0 was found to provide the best compromise between sensitivity and false detections.

4.1 Velocity estimation

An attempt to estimate the shower meteors' velocity was made for radiants whose activities exceeded the detection threshold. A histogram of meteor velocities in a 4° wide band perpendicular to the active radiant was constructed. Modelling similar to that described in Love & Brownlee (1990) indicated that micrometeoroid deceleration is slight in the initial stages of ablation, only becoming severe

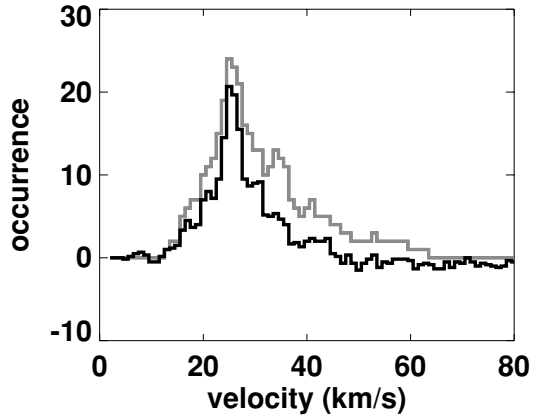

Figure 1. Meteor velocities for the Day χ Sagittariids shower detected on 2006 January 11 at Davis Station, before subtraction of a background estimate (light) and after (dark).

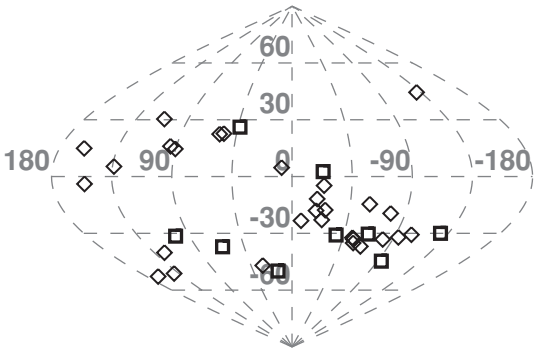

Figure 2. Locations of detected showers at peak strength in equatorial (J2000) (RA–Dec) coordinates. Diamonds are documented showers and squares are new discoveries. Overlapping showers are distinguished by date of occurrence and/or velocity.

just prior to the cessation of ionization. In order to minimize the effect of atmospheric deceleration, only meteors above the daily peak detection height were used for velocity estimation.

This histogram still contained a distribution of background meteor velocities, so an estimate of the background was constructed using the velocities in bands corresponding to radiants at the same declination, but spaced at $\pm 90^\circ$ right ascension from the active radiant. Holdsworth et al. (2008) suggest constructing a background estimate from a single radiant much closer to the target radiant, but given the large number of multiple filament shower complexes seen, it was decided that this produced an undue risk of including members of the target shower's family in the background estimate.

The estimate of the background velocity distribution was then subtracted from the target radiant's velocity histogram, leaving an estimate of the shower meteors' velocities, as seen in Fig. 1. Once isolated, the peak remaining in the histogram was fitted with a Gaussian curve, with the centre of the curve being the estimate of the shower's relative velocity. Velocity peaks containing less than 50 meteors were rejected, due to the possibility of very weak showers' velocity profiles being overwhelmed by the sporadic background, even with the subtraction of a background estimate.

4.2 Detected meteor showers

Using the above criteria, 607 active radiants were logged, each representing a distinct shower occurring during a 24-h period. Of these, estimates of velocity was able to be made for 530. Uncertainty in the velocity estimate ranged from 5 to 25 per cent, the upper limit being due to rejection criteria. The larger uncertainty velocity estimates are due not to uncertainties in individual measurements, but rather statistical uncertainty in the distribution of suspected shower meteor velocities in lower SNR showers. Most shower velocity estimates had an uncertainty of about 10 per cent. This is consistent with the inherent uncertainty of individual meteor velocities obtained using the Fresnel transform method (Campbell & Elford 2006). In this light, meteor showers provide a means to estimate the accuracy of different meteor radar velocity determination techniques.

After the automated detection and acceptance–rejection process, the daily detections were manually sorted into distinct showers. A shower was considered as being confirmed if it lasted multiple days with consistent radiant drift, occurred in the same location at the same solar longitude in different years, or had a single day detection with a SNR in excess of 2.5.

Identification of showers was made using a combination of sources, as there is no single comprehensive catalogue of known meteor showers. The International Astronomical Union maintains a simple data base of shower locations, including over 300 reported and named showers (Slovak Academy of Sciences 2007). Gary Kronk's Meteor Showers Online (Kronk 2008), the extension of his previous published volume on the matter, provides a detailed description of most showers and lists a number of showers only detected by radar or forward scatter methods. Jennisken's list of visual showers (Jenniskens 1994) and Cook's compilation (Cook 1973) served to further refine particular showers' identities. The Canadian Meteor Orbit Radar has produced a detailed high-precision catalogue of meteor showers (Brown et al. 2007), but the northern hemisphere location of the observing radar limited its utility for this survey.

The detected showers comprised 37 different shower systems, summarized in Fig. 2 and listed in more detail in Table 1. Of these, nine were not present in any of the catalogues used for identification, not including showers that represented a significant temporal lengthening of already recognized shower systems. Of the unlisted showers, one located at 16°, -50° has been described earlier by Holdsworth et al. (2008), which used some of the same data from Davis Station in the analysis.

An undocumented shower located at 336.7°, 2.6° on the date of maximum activity, seen in Fig. 3, appears to be a secondary filament of the η Aquariid stream. Not only does the undocumented shower stay in close proximity at a fixed position relative to the η Aquariid radiant throughout its duration, both showers' daily velocity estimates are in good agreement, typically within 1 km s^{-1} of each other.

The seemingly high discovery rate of $\sim$24 per cent is due to a combination of factors relating to the methods used and existing meteor catalogues. The radars used are designed to exploit the specular reflection condition of very weak, subvisual meteors produced by objects with a typical initial diameter less than 1 mm. This results in a detection rate in excess of 12 000 meteors per day, sometimes exceeding 25 000 per day. These high counts, combined with the sensitivity of the Jones & Jones convolution method to narrow sources, make it possible to detect weak showers that might otherwise be lost in the sporadic background. Jones & Jones (2006) and Holdsworth et al. (2008) showed that the Jones & Jones weighting function is extremely sensitive to narrow shower sources, even when buried in a diffuse background.

Table 1. Meteor showers detected at Darwin, Australia (A) and Davis Station, Antarctica (B) during 2006–2007. First date is the earliest date of detection and last date is the latest date that the shower was detected. Peak $\lambda_\odot$ is the solar longitude on the day of a shower's maximum activity. Velocities are as estimated on the date of maximum activity.

Shower name	First date	Last date	Peak $\lambda_\odot$	Peak RA	Peak Dec.	RA drift ($^\circ$day^{-1})	v (km s^{-1})	Δv (km s^{-1})
α Piscis Australids (B)	July 24	July 29	120.9	335.9	−22.9	3.39	39.8	4.2
α Puppids[a] (B)	January 6	December 30	276.3	140.9	−51.2	0.41	40.2	5.8
Day χ Sagittariids[a] (B)	January 2	January 11	286.7	281.7	−19.5	0.87	26.4	3.4
Day κ Leonids[a] (A)	September 22	September 28	174.0	161.0	14.9	0.23	40.0	5.9
Day Sagittariids–Capricorinids[a] (B)	January 9	February 21	299.2	305.3	−33.1	0.49	25.6	3.0
η Aquariids[a] (A, B)	April 29	May 14	39.8	335.9	−4.8	0.60	60.6	7.9
η Carinids (B)	January 4	January 15	288.0	165.8	−52.8	1.00	37.7	4.9
Geminids (A)	December 2	December 13	261.0	110.8	30.4	1.11	35.1	2.1
July Phoenecids (A, B)	July 4	July 21	107.8	32.1	−47.0	1.38	39.2	4.3
Northern δ Aquariids (A)	July 23	July 31	117.3	334.0	−17.7	0.77	40.7	4.1
Northern Taurids (A)	November 8	November 8	225.8	55.3	22.7	–	29.2	2.3
November Orionids (A)	November 22	December 4	245.8	90.3	14.6	0.68	41.7	4.8
Orionids (A)	October 15	October 31	207.9	94.7	16.0	0.60	60.5	9.3
ϕ Sagittariids (B)	June 5	June 25	88.5	278.9	−33.2	−0.03	26.8	3.6
Piscis Austrinids (A, B)	July 25	August 14	126.9	352.7	−23.3	1.40	38.7	5.2
Quadrantids[a] (A)	January 3	January 4	282.9	229.3	44.5	4.41	40.9	3.0
Sagittariids (A, B)	June 8	June 13	75.1	304.1	−35.1	−0.10	36.4	3.6
Sextantids[a] (A, B)	September 26	October 4	188.1	155.7	−3.9	0.56	32.7	2.7
σ Hydrids (A)	November 12	November 12	229.6	133.9	5.3	–	–	–
Southern δ Aquariids (A, B)	July 17	August 14	120.9	341.1	−18.0	0.54	39.2	3.9
Southern ι Aquariids (A)	July 23	August 7	121.9	340.8	−11.8	0.57	40.1	3.7
Southern June Aquilids (B)	June 13	June 13	77.0	296.1	−36.9	–	34.5	7.2
Southern May Ophiuchids (B)	May 24	May 24	58.1	256.1	−30.7	–	28.5	6.8
Southern Piscids (A)	September 10	September 10	162.3	7.8	4.7	–	32.2	6.6
τ Capricorinids (B)	July 17	July 19	109.4	299.9	−14.6	0.55	27.6	4.8
θ Ophiuchids (A, B)	June 2	June 21	74.4	266.1	−32.1	−0.01	27.5	4.2
ζ Perseids[a] (A)	June 3	June 15	67.4	58.6	22.4	0.00	31.4	7.1
ζ Puppids[a] (B)	November 3	November 6	222.8	125.0	−40.2	0.40	35.8	4.6
Unknown 1[a] (B)	January 14	January 18	297.9	293.9	−30.4	−0.33	26.1	4.3
Unknown 2[a] (B)	February 6	February 9	319.5	231.7	−30.0	−2.61	54.8	10.8
Unknown 3[a] (A)	March 19	March 31	358.7	266.0	−44.7	0.06	57.4	8.1
Unknown 4[a] (B)	April 29	April 30	34.7	16.2	−49.9	−0.80	42.9	3.0
Unknown 5[a] (A)	April 29	May 14	40.5	336.7	2.6	0.92	60.3	8.6
Unknown 6[a] (A)	June 10	June 19	75.1	43.4	26.1	−0.01	39.6	4.4
Unknown 7 (B)	July 1	July 10	102.1	321.6	−30.9	0.78	35.2	5.2
Unknown 8 (B)	September 9	September 9	161.6	65.2	−37.1	–	38.3	9.6
Unknown 9[a] (B)	October 8	October 21	198.9	102.2	−31.5	−0.48	35.6	5.9

[a]These are daytime showers (radiants within 90° of the Sun).

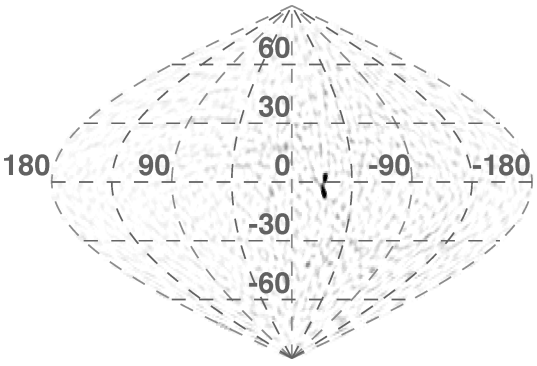

Figure 3. Darwin radar radiant activity map for 2007 May 6. The η Aquariid shower is visible as a dark spot below the equator, with an undocumented shower just above the equator.

Most established showers' observations were made primarily using visual or photographic methods. These methods, while capable of producing high-precision radiant information are reliant on larger, less frequent luminous meteors and depend on clear viewing conditions. Additionally, visual methods completely exclude any showers that occur during daylight. Defining a daylight shower to be one whose radiant lies within 90° of the Sun, seven out of the nine undocumented showers were daytime showers.

5 CALCULATING ORBITAL ELEMENTS

Having detected not only the radiant of individual meteor streams but also the relative intercept velocity of the incoming particles, the natural application of the data is to calculate the orbital parameters of the detected meteoroids.

Before the problem can be tackled, the velocity of the meteors must be corrected for the acceleration undergone during the Earth infall process. For a particle at initial velocity v_∞ outside the Earth's

sphere of influence, the atmospheric entry velocity v_a at a distance r_e from Earth's centre of mass is given by

$$v_\infty = \sqrt{v_a^2 - \frac{2GM_e}{r_e}}, \tag{2}$$

where M_e is Earth's mass and G is the gravitational constant.

The vis-viva equation is the first stop in solving for an object's orbital elements

$$v = \mu\sqrt{\frac{2}{r} - \frac{1}{a}} \tag{3}$$

which can be solved for a, the orbit's semimajor axis. μ, the standard gravitational parameter, is given by $G\,\mathrm{M}_\odot$, where $\mathrm{M}_\odot$ is the mass of the Sun. The distance of the object from the Sun, r is the Earth's distance from the Sun at the time of detection for meteors, which is well known at any given time. After adding the Earth's heliocentric velocity to the relative intercept velocity to obtain the stream's true orbital velocity, three more equations taken from elliptical geometry and Kepler's relations can then be solved to provide the remaining elements:

$$rv_\perp = \sqrt{\mu p}, \tag{4}$$

$$e = \sqrt{1 - \frac{p}{a}} \tag{5}$$

and

$$r = \frac{p}{1 + e\cos(\theta)}, \tag{6}$$

where $v_\perp$ is the stream's velocity normal to the radial vector towards the Sun, p is the *semi-latus rectum* of the orbit, e is the orbit's eccentricity and θ is the argument of the body's position, measured from the perihelion.

Equation (6) can be solved for the stream's argument, but the angle θ produced is only the angle between the perihelion and the stream's current position. To find the true anomaly, which will also yield the argument of the perihelion from the ascending node, the radial component of velocity v_r is found. For outbound objects where $v_r > 0$, the argument of the perihelion, ω, is just θ. For inbound objects with $v_r < 0, \omega = \theta + 180^\circ$.

Using the geometry of Earth's known velocity vector and the meteor streams' estimated velocity vector, inclination is found as the arcsine of the angle between the Earth's $v_\perp$ and the meteor stream's $v_\perp$.

6 METEOR STREAM ORBITS

Orbits were successfully calculated for 31 of the detected showers, which are detailed in Table 2. These include eight of the nine of the newly discovered systems. In addition, the orbits of another five showers were calculated, but these estimates suffered from

Table 2. Calculated orbital elements for detected showers, made from combined daily estimates. Ω = argument of the ascending node on the day of peak activity, ω = argument of the perihelion from the ascending node, a = semimajor axis, e = eccentricity, i = inclination relative to the plane of Earth's orbit. Errors indicate 95 per cent confidence.

Shower name	Ω	ω	$\Delta\omega$	a (au)	Δa (au)	e	Δe	i	Δi
α Piscis Australids	306.4	138.0	6.4	2.82	1.31	0.936	0.030	32.3	23.6
α Puppids	95.0	82.2	40.2	1.70	0.12	0.432	0.046	71.2	1.7
Day χ Sagittariids	287.2	282.3	2.1	1.86	0.09	0.743	0.009	2.9	0.2
Day κ Leonids	179.5	325.6	2.8	2.72	1.01	0.955	0.009	20.0	2.3
Day Sagittariids–Capricorinids	119.7	273.6	5.0	2.03	0.10	0.734	0.014	9.3	0.2
η Aquariids	45.3	289.2	1.8	1.46	0.07	0.675	0.018	168.3	0.5
η Carinids	108.5	201.0	55.0	0.95	0.01	0.043	0.009	74.0	0.8
Geminids	261.5	143.2	2.6	1.32	0.09	0.884	0.004	18.0	0.5
July Phoenecids	293.3	63.8	4.3	1.38	0.07	0.346	0.035	73.5	0.6
Northern δ Aquariids	302.8	147.5	1.0	2.50	0.16	0.960	0.003	17.4	1.5
November Orionids	66.3	140.8	1.7	4.52	1.30	0.962	0.007	21.7	1.7
Orionids	24.4	108.8	7.8	1.42	0.45	0.617	0.113	163.0	0.8
ϕ Sagittariids	273.9	103.2	3.2	2.00	0.11	0.762	0.014	8.3	0.3
Piscis Austrinids	312.4	148.2	4.4	1.43	0.15	0.911	0.018	36.7	8.0
Quadrantids	283.4	197.3	13.8	1.72	0.10	0.437	0.023	72.4	0.7
Sagittariids	260.6	155.6	1.3	1.00	0.04	0.905	0.008	46.1	3.0
Sextantids	8.6	326.1	1.7	1.09	0.03	0.858	0.007	23.9	1.0
Southern δ Aquariids	306.4	148.3	1.2	1.71	0.10	0.933	0.004	32.9	1.7
Southern ι Aquariids	307.3	156.4	1.5	1.64	0.06	0.962	0.003	12.0	0.7
τ Capricorinids	114.9	98.1	1.7	2.59	0.29	0.807	0.031	5.2	0.7
θ Ophiuchids	263.7	106.2	3.9	2.04	0.13	0.780	0.012	7.7	0.7
ζ Perseids	76.8	305.8	9.8	1.70	0.20	0.831	0.048	5.0	2.3
ζ Puppids	43.3	236.5	8.3	1.10	0.05	0.151	0.035	67.4	0.4
Unknown 1	118.4	278.2	10.3	1.91	0.10	0.735	0.031	8.5	1.2
Unknown 2	140.5	333.6	20.1	0.79	0.07	0.364	0.125	149.0	6.2
Unknown 3	185.1	–	–	1.01	0.06	0.307	0.253	147.5	9.2
Unknown 4	219.4	244.6	3.6	2.28	0.33	0.657	0.043	73.9	1.4
Unknown 5	45.0	285.6	3.1	1.67	0.13	0.707	0.018	152.2	0.9
Unknown 6	80.6	335.2	1.5	1.43	0.07	0.949	0.004	31.1	2.2
Unknown 7	288.5	140.8	1.5	1.40	0.11	0.874	0.012	30.4	2.7
Unknown 9	21.8	–	–	1.14	0.04	0.176	0.021	66.5	2.7

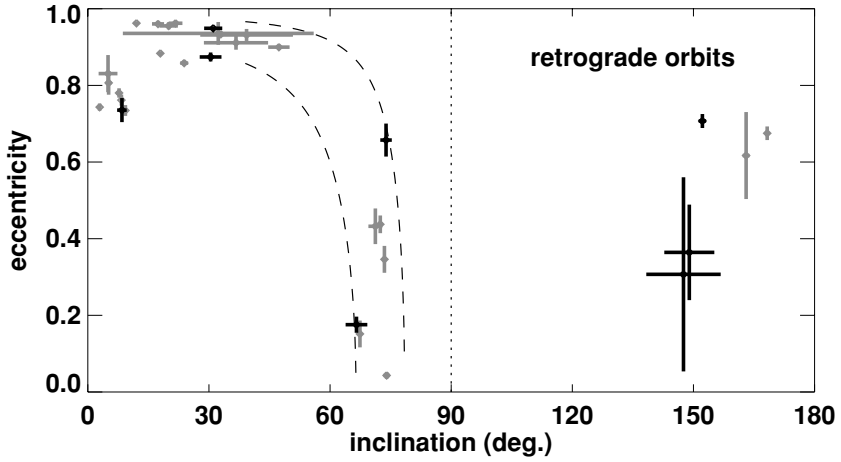

Figure 4. Orbital elements calculated for detected showers, with newly discovered showers plotted in dark and documented showers in grey. Dashed lines are contours of Kozai resonance for $H_K = 0.4$ (left) and $H_K = 0.2$ (right). Error bars represent 95 per cent confidence.

excessive uncertainties, owing to having only a single day's detection for each of the showers. Orbital elements could not be calculated for an additional shower due to an inability to resolve the shower velocity.

The argument of the perihelion from the ascending node could not be resolved for two showers, both of which have very low-eccentricity orbits. Additionally, the α Puppids, η Carinids and the shower designated unknown 2 in 1 suffered from large errors in ω. Given these showers' lower eccentricity orbits, it is unsurprising that this parameter suffers from excessive uncertainty.

Looking at the distribution of orbital elements shown in Fig. 4, there appears to be four major classes of meteor stream orbits in the data. Inclinations of greater than 90° correspond to retrograde orbits, a notable example being comet 1P/Halley, which is the source of two detected and well-known showers around $i = 165°, e = 0.650$, the η Aquariids and the Orionids (Kronk 2008). The newly detected shower whose radiant and velocity indicate it to be a secondary filament of the η Aquariid stream occupies a similar orbit, but with a greater angle between it and the ecliptic plane. An additional two undocumented streams were found to have retrograde orbits with much lower eccentricities and higher inclinations than the Halley-based streams.

In terms of inclination and eccentricity, the two undocumented retrograde streams near $i = 150°, e = 0.350$ appear to share quite similar orbits, but their ascending nodes are separated by 46°. This indicates that while the two orbits may share the same parent body, they are not individual detections of the same stream. Any scenario involving a common parent body would require a significant precession of the body's ascending node between the production of the two streams. Such is the case of the Orionids and the η Aquariids, whose ascending nodes were found to have a mean separation of 23°.

With inclinations in excess of 60°, seven different meteor stream orbits (two undocumented) are possibly the product of the Kozai mechanism. Kozai found that during orbital perturbations, high-eccentricity, low-inclination orbits can be converted to low-eccentricity, high-inclination orbits as the quantity $H_K = \sqrt{1 - e^2}\cos(i)$ is conserved, which is a consequence of the conservation of angular momentum in the perturbative process (Murray & Dermott 1999). As a result, a number of highly inclined, nearly circular orbits can be seen in Fig. 4 lying along contours of H_K that connect with orbital regimes normally associated with high-eccentricity cometary orbits.

Two general populations of low-inclination, high-eccentricity orbits are evident. The first, with eccentricities in excess of 0.85 and inclinations centred around 30°, consists primarily of the Aquariid and Piscis Austrinid complexes, in addition to the Geminids, Daytime κ Leonids, November Orionids, Sagittariids, Sextantids and two undocumented showers. Of particular interest is the complex of showers comprised of the Southern δ and ι Aquariids, the α Piscis Australids and the Piscis Austrinids. With all occurring in the same region of the sky during July–August and with similar orbital elements, it seems likely that these showers are all separate filaments of debris related to a common source object. Brown et al. (2007) also noted this relation and extended it to include the Taurid complex, which was not detected in this survey.

A second, more compact group of orbits is centred around $e = 0.75$ and $i = 10°$ is comprised of the Daytime χ Sagittariids, Daytime Sagittariid–Capricorinids, ϕ Sagittariids, τ Capricorinids, θ Ophiuchids, ζ Perseids and one undocumented shower.

Notably absent from the results were any streams with hyperbolic orbits. Such a shower would be particularly rare given that it would be of extra-solar origin and only occur once, as the Solar system passed through the debris stream. Additionally, the current implementation of the Fresnel transform method for velocity determination breaks down around 80 km s^{-1} due to an inadequate sampling frequency (Holdsworth et al. 2007). Given a geocentric solar escape velocity of 72 km s^{-1}, even relatively slow extra-solar meteors would be difficult to obtain velocity estimates for.

Further complicating matters, very high velocity meteoroids will ablate at higher altitudes, which may be beyond the radar's high-altitude cut-off. The effective initial radius of a meteor's column of ionization increases with the altitude of the meteor's ablation (Jones 1995), which produces progressively weaker signal return with meteor altitude due to destructive interference within the trail. Also increasing with altitude is the ambipolar diffusion coefficient, which is inversely proportional to the decay time of an underdense meteor radar echo for a particular frequency (McKinley 1961). As a result, at higher altitudes, a pulsed radar's repetition frequency may be insufficient to detect short-duration echoes.

7 CONCLUSIONS

Using single station interferometric meteor radar observations collected during 2006–2007 at Davis Station, Antarctica and Darwin, Australia, 37 distinct meteor showers were detected, including nine

not in commonly used catalogues. Of the newly discovered showers, seven occur during the daytime, making radio the only possible detection method.

Using the apparent radiants and velocity estimates of the detected showers, the orbits of 31 meteor streams were successfully calculated. These orbits were found to occupy four broad categories, and there were a number of instances suggestive of a common origin of different meteor streams.

The specular reflection condition of underdense meteors would ordinarily be a limitation in determining meteor shower trajectories, but using the Jones & Jones convolution method, an interferometric meteor radar can be a valuable tool in meteor astronomy. This method exemplifies 'science of opportunity' that can be done with data collected for entirely different purposes.

Given the relative simplicity of the process and the number of similar meteor radar systems operating around the world, this work could easily be extended to a global meteor shower detection network, requiring only the input of a few observed parameters into a central data base for analysis.

ACKNOWLEDGMENTS

This research was conducted with financial support from ASAC grant 2529 and ARC grants DP0878144 and DP0558361.

REFERENCES

Baggaley W. J., Bennett R. G. T., Steel D. I., Taylor A. D., 1994, Q. J. R. Astron. Soc., 35, 293
Brown P., Weryk R. J., Wong D. K., Jones J., 2007, Icarus, 195, 317
Campbell L., Elford W. G., 2006, Planet. Space Sci., 54, 317
Caswell R. D., McBride N., Taylor A., 1995, Int. J. Impact Eng., 17, 139
Cook A. F., 1973, Proc. IAU Colloq. 13, Evolutionary and Physical Properties of Meteoroids, NASA SP-319
Davies J. G., Gill J. C., 1960, MNRAS, 121, 437
Dycus R. D., Richardson J., 1969, J. Spacecraft, 6, 1070
Elford W. G., 2004, Atmos. Chem. Phys., 4, 911
Holdsworth D. A., 2005, Radio Sci., 40, RS6010
Holdsworth D. A., Reid I. M., Cervera M. A., 2004, Radio Sci., 39, RS5009
Holdsworth D. A., Elford W. G., Vincent R. A., Reid I. M., Murphy D. J., Singer W., 2007, Ann. Geophys., 25, 385
Holdsworth D. A., Murphy D. J., Reid I. M., Morris R. J., 2008, Adv. Space Res., 42, 143
Jenniskens P., 1994, Astron. Astrophys., 287, 990
Jones W., 1995, MNRAS, 275, 812
Jones J., Jones W., 2006, MNRAS, 367, 1050
Jones J., Webster A. R., Hocking W. K., 1998, Radio Sci., 33, 55
Jones J., Brown P., Ellis K. J., Webster A. R., Campbell-Brown M., Krzemenski Z., Weryk R. J., 2005, Plan. Space Sci., 53, 423
Kronk G. W., 2008, Meteor Showers Online, http://meteorshowersonline.com/
Love S. G., Brownlee D. E., 1990, Icarus, 80, 26
McKinley D. W. R., 1961, Meteor Science and Engineering. McGraw–Hill, New York
Murray C. D., Dermott S. F., 1999, Solar System Dynamics. Cambridge Univ. Press, Cambridge
Slovak Academy of Sciences, 2007, IAU Meteor Data Center, http://www.astro.amu.edu.pl/∼jopek/MDC2007/
Weiss A. A., 1958, MNRAS, 120, 387

This paper has been typeset from a TEX/LATEX file prepared by the author.